# ROBUST PHASE DIFFERENCE ESTIMATION OF TRANSIENTS IN HIGH NOISE LEVELS

1st Oskar Keding
*Centre for Mathematical Sciences*
*Lund University*
Lund, Sweden
oskar.keding@matstat.lu.se

2st Maria Sandsten
*Centre for Mathematical Sciences*
*Lund University*
Lund, Sweden
maria.sandsten@matstat.lu.se

***Abstract*—This paper presents the Reassignment Vector Phase Difference Estimator (RVPDE), which gives noise robust relative phase estimates of oscillating transient signals in high noise levels. Estimation of relative phase information between signals is of interest for direction of arrival estimation, source separation and spatio-temporal decoding in neurology as well as for soundscape analysis. The RVPDE relies on the spectrogram reassignment vectors which contains information of the time-frequency local phase difference between two transient signals. The final estimate, which is robust to high noise levels, is given as the median over the local time-frequency area. The proposed technique is shown to outperform state-of-the-art methods in simulations for high noise levels. A discussion on the statistical distribution of the estimates is also presented, and finally an example of phase difference estimation of visually evoked potentials measured from electrical brain signals is shown.**

***Index Terms*—time-frequency reassignment, oscillating transient signals, low SNR, phase estimation, EEG**

## I. Introduction

Oscillating transient signals are analyzed in many application areas. They are the key structures in ultrasound analysis, seismic wave detection, vibration signal characterization, and classification of animal communication signals, e.g. sounds from birds, bats, and dolphins. Further, transients are significant signatures in classification of electrical signals measured form the human brain, the electroencephalogram (EEG) signals.

However, such measurements are typically very noisy and hard to analyze. Time-frequency (TF) representations serve as the common ground to be optimized for the extraction of relevant information. State-of-the-art methods aim at increased concentration of TF components and suppression of cross-terms using the quadratic class of TF representations [1]. Moreover, the TF reassignment and synchrosqueezing methods are well known techniques for sharpening and increasing visualization of TF representations, which also have been explored for different applications [2]–[7]. We have shown that a Gaussian envelope oscillatory signal can achieve perfect TF localization, using a scaled and matched reassignment technique [8]–[10].

In many fields of audio and soundscape analysis, estimation of phase differences is needed for directional estimation and source separation [11]. Phase synchrony or relative phase estimations are also of extremely important to decode spatio-temporal information in multiple areas of neurology [12], [13]. Scalp-recorded EEG signals have low signal-to-noise ratios (SNRs), and methods robust to high disturbances are much needed. We have invented a phase difference estimation method for oscillatory components in multi-channel EEG signals [14], [15]. However, this technique relies on known information of the component envelope shape and has also shown to be sensitive to high noise levels. In a recent paper, we presented a novel approach to phase difference estimation for Gaussian envelope oscillatory components, based directly on the reassignment vector information [16]. As a continuation, by further exploring the theory and adding a final step of a median filter for noise robustness, this paper presents a method for estimating phase difference between short oscillatory signals with arbitrary envelope shape, specifically for low SNRs.

Preliminaries of the matched reassigned spectrogram and cross-spectrogram are presented in section 2 and 3. Section 4 proposes the novel technique of the Reassignment Vector Phase Difference Estimator (RVPDE), which is first evaluated as an estimator over TF-bins. The method is also compared to contemporarily used methods for estimation of relative phase difference of TF components in signal pairs in section 5. Penultimately, section 6 presents results of method application on a set of visually evoked potentials (VEPs) from measured EEG and final conclusions are given in section 7.

## II. Reassigned Spectrogram

An oscillating transient signal $x(t)$ is defined as

$$x(t) = g(t - t_0)e^{i(\omega_0 t + \phi_0)} \tag{1}$$

where $g(t)$ is the signal envelope, $t_0$ the time location, $\omega_0$ the oscillating frequency and $\phi_0$ the phase. The short time Fourier transform (STFT), $F_x^h(t, \omega)$, with a window function $h(t)$ is

$$F_x^h(t, \omega) = \int x(s)h^*(s - t)e^{-i\omega s}ds \tag{2}$$

where $t$ denotes time, $\omega$ denotes angle frequency and $^*$ complex conjugate. Integrals are assumed to range between $-\infty$

Thanks to the ELLIIT strategic research programme for funding.

and $\infty$ unless stated otherwise. To improve the visualisation of the spectrogram

$$S_x^h(t,\omega) = F_x^h(t,\omega)\left(F_x^h(t,\omega)\right)^* \tag{3}$$

reassignment relocates energy to the energy mass centre of signal components according to

$$RS_x^h(t,\omega) = \iint S_x^h(s,\xi)\delta\left(t-\hat{t}_x(s,\xi),\omega-\hat{\omega}_x(s,\xi)\right)dsd\xi \tag{4}$$

using the two-dimensional Dirac function. Vector functions for energy relocation $\hat{t}_x(t,\omega)$ and $\hat{\omega}_x(t,\omega)$ are defined as

$$\hat{t}_x(t,\omega) = t + c_t\Re\left(\frac{F_x^{th}(t,\omega)}{F_x^h(t,\omega)}\right) \tag{5}$$

$$\hat{\omega}_x(t,\omega) = \omega - c_\omega\Im\left(\frac{F_x^{\frac{dh}{dt}}(t,\omega)}{F_x^h(t,\omega)}\right) \tag{6}$$

where $\Re(\bullet)$ and $\Im(\bullet)$ represent the real and imaginary parts, and $F_x^{th}(t,\omega)$,$F_x^{\frac{dh}{dt}}(t,\omega)$ are the STFTs of the signal $x(t)$, with $t\cdot h(t)$ and $dh(t)/dt$ as window functions. A matching window function to the signal envelope, $h(t) = g(-t)$, together with a suitable choice of constants $c_t$ and $c_\omega$ result in perfect relocations to time and frequency energy centres for arbitrarily shaped components, [8]–[10].

## III. Reassigned Cross-Spectrogram

Expanding the concepts of reassignment to multi-dimensional data, a pair of signals $y_1(t)$ and $y_2(t)$ is considered, containing a transient oscillating component of shape $g(t)$ phase-shifted between signals, i.e.

$$y_1(t) = e^{i\Delta\phi}x(t), \quad y_2(t) = x(t) \tag{7}$$

Although left out in this paper, components with non-equal amplitudes can also be considered, by estimating scaling constants for reassignment vectors as in [15]. A reassigned cross-spectrogram between these two signals is defined as

$$RS_{y_1,y_2}^h(t,\omega) = \iint |S_{y_1,y_2}^h(s,\xi)|\delta\left(t-\hat{t}_{y_1,y_2}(s,\xi),\omega-\hat{\omega}_{y_1,y_2}(s,\xi)\right)dsd\xi \tag{8}$$

where $S_{y_1,y_2}^h(t,\omega) = F_{y_1}^h(t,\omega)\left(F_{y_2}^h(t,\omega)\right)^*$. The reassignment vectors are expanded to contain mixed information about both STFTs of signals as

$$\hat{t}_{y_1,y_2}(t,\omega) = t + c_t\Re\left(\frac{F_{y_1}^{th}}{F_{y_2}^h} + \frac{F_{y_2}^{th}}{F_{y_1}^h}\right) \tag{9}$$

$$\hat{\omega}_{y_1,y_2}(t,\omega) = \omega - c_\omega\Im\left(\frac{F_{y_1}^{\frac{dh}{dt}}}{F_{y_2}^h} + \frac{F_{y_2}^{\frac{dh}{dt}}}{F_{y_1}^h}\right) \tag{10}$$

where the $(t,\omega)$ notation is dropped in the STFTs for conciseness [14], [16].

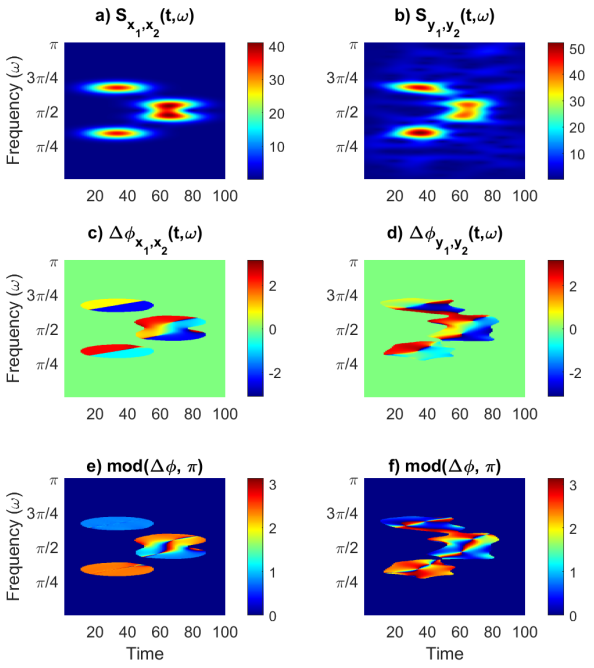


Fig. 1. The cross spectrogram for a pair of noise free and noisy ($\sigma_e = 2$) signals with four oscillatory components are shown in a and b respectively. The resulting $\widehat{\Delta\phi}(t,\omega)$ estimates are shown in c,d and their modulus with regard to $\pi$ are shown in e,f. In total, the signal has four components with $t_0 = 33, 33, 66, 66$, $\omega_0 = \pi/3,\ 2\pi/3,\ 11\pi/24,\ 13\pi/24$ and $\Delta\phi = 3\pi/4, \pi/4, \pi/4, 3\pi/4$ with Gaussian shaped envelopes ($\sigma = 12$). The spectrogram was calculated with a Gaussian window ($\lambda = 12$).

## IV. Phase Difference Estimation

To present the Reassignment Vector Phase Difference Estimator (RVPDE) as a method of relative phase difference between signal components, the phase information inherent in reassignment vectors $F_x^{th}/F_x^h$ is inquired. As a point of novelty, one can utilise, regardless of envelope $g(t)$, the fractions in the second addends of (9) and (10) and rearrangment of terms to construct estimates for the phase difference of the signals over time and frequency. This can be done without calculating any new STFTs or quotients as

$$\begin{aligned} CR(t,\omega) &= \Re\left(\frac{F_{y_1}^{th}}{F_{y_2}^h} + \frac{F_{y_2}^{th}}{F_{y_1}^h}\right) = \Re\left(\frac{F_x^{th}}{F_x^h}\right)2\cos(\Delta\phi) \\ CI(t,\omega) &= \Im\left(\frac{F_{y_1}^{\frac{dh}{dt}}}{F_{y_2}^h} + \frac{F_{y_2}^{\frac{dh}{dt}}}{F_{y_1}^h}\right) = \Im\left(\frac{F_x^{\frac{dh}{dt}}}{F_x^h}\right)2\cos(\Delta\phi) \end{aligned} \tag{11}$$

$$\begin{aligned} SR(t,\omega) &= \Im\left(\frac{F_{y_1}^{th}}{F_{y_2}^h} - \frac{F_{y_2}^{th}}{F_{y_1}^h}\right) = \Re\left(\frac{F_x^{th}}{F_x^h}\right)2\sin(\Delta\phi) \\ SI(t,\omega) &= \Re\left(\frac{F_{y_1}^{\frac{dh}{dt}}}{F_{y_2}^h} - \frac{F_{y_2}^{\frac{dh}{dt}}}{F_{y_1}^h}\right) = -\Im\left(\frac{F_x^{\frac{dh}{dt}}}{F_x^h}\right)2\sin(\Delta\phi) \end{aligned} \tag{12}$$

Combining expressions (11) and (12) forms an angular estimate of a complex quantity in each STFT bin, carrying infor-

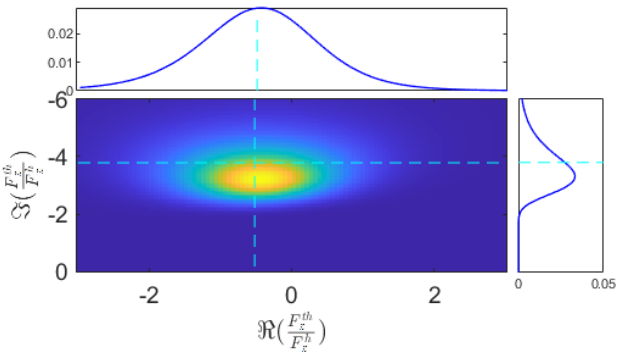


Fig. 2. shows the complex-valued distribution of $F_z^{th}/F_z^h$ at the TF bin $(t_0, \omega_0 + 30\pi/512)$, for a one-component signal $z(t) = x(t) + n(t)$ with TF-centre $(t_0, \omega_0)$ where $n(t)$ is white noise with $\sigma_e = 1$. The signal $z(t)$ has component centre $(t_0, \omega_0) = (100, \pi/4)$, $\sigma = 12$, and normalized power over $\pm 3\sigma$ of the centre. STFTs were calculated with a Gaussian window $h$ with $\lambda = 4$. The complex valued distribution is shown together with the marginal distributions over $\Re(F_z^{th}/F_z^h)$ and $\Im(F_z^{th}/F_z^h)$. The dashed cyan lines marks the noise-free value $F_x^{th}/F_x^h$.

mation about the phase difference of the transient oscillating component in the two signals,

$$\begin{aligned}
&(CR(t,\omega) + CI(t,\omega)) + i\,(SR(t,\omega) - SI(t,\omega)) = \\
&(\Re\left(\frac{F_x^{th}}{F_x^h}\right) + \Im\left(\frac{F_x^{\frac{dh}{dt}}}{F_x^h}\right))2\cos(\Delta\phi) + \\
&(\Re\left(\frac{F_x^{th}}{F_x^h}\right) + \Im\left(\frac{F_x^{\frac{dh}{dt}}}{F_x^h}\right))2i\sin(\Delta\phi) = \\
&K(t,\omega)(\cos(\Delta\phi) + i\sin(\Delta\phi)) = K(t,\omega)e^{i\Delta\phi}
\end{aligned} \tag{13}$$

Then $\widehat{\Delta\phi}(t,\omega) = \arg(K(t,\omega)e^{i\Delta\phi})$ results in estimates of phase difference over TF-bins for signals also possibly containing multiple arbitrarily formed TF-components in the TF-domain. An example of phase estimation of a noiseless multicomponent signal for oscillatory signals with Gaussian envelopes

$$g(t) = e^{-\frac{t^2}{2\sigma^2}} \tag{14}$$

is shown in Figure 1. Figure 1a and b show the cross-spectrogram of signals containing four components with different spectral and temporal centres in a noiseless and noisy $(\sigma_e = 2)$ scenario respectively. Figure 1c and d show the angular phase difference estimate between signals. The method is clearly successful in calculating separate $\Delta\phi$ in high levels of added noise, for non-overlapping TF components. Figure 1c and d illustrates one short-coming, that $K(t,\omega)$ takes on negative values, which creates a $\pi$ angular rotation in the estimates. This is solved by taking the modulus of the angle values $\widehat{\Delta\phi_m}(t,\omega) = \text{mod}(\widehat{\Delta\phi}(t,\omega), \pi)$ restricting estimates to an expected range $\Delta\phi \in [0, \pi]$, as in Figure 1 e and f.

A significant improvement with this method is that the estimation in each bin makes no assertion regarding the shape of the components as long components in each channel share envelope $g_1(t) = g_2(t)$. The applied window shape $h(t)$ could be arbitrarily chosen and is for now chosen to be Gaussian defined from

$$h(t) = 1/(\pi^{1/4}\sqrt{\lambda})e^{-\frac{t^2}{2\lambda^2}} \tag{15}$$

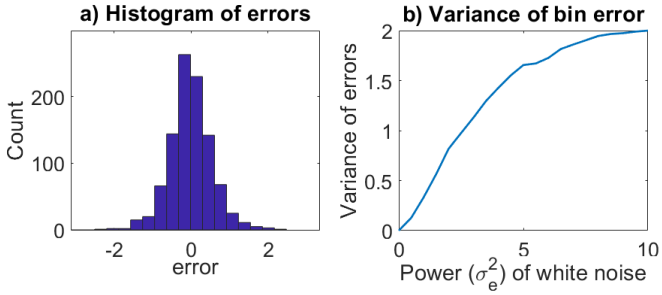


Fig. 3. (a) shows the distribution of errors for $\widehat{\Delta\phi}(t,\omega)$, before modulus and median is taken, in the TF bin $(t_0, \omega_0 + 10\pi/512)$ where $(t_0, \omega_0)$ is the centre point of the components. One can see this the estimate is approximately normal distributed. (b) shows the variance relation of the phase difference errors to increasing signal noise variances $\sigma_e^2$ in the same bin.

The quality of $\widehat{\Delta\phi_m}(t,\omega)$ for a signal depends on the ratio of signal to noise for Fourier transforms in each bin. For a certain component one can use multiple methods to extract a robust single estimate of phase difference between channels for a chosen component $a$. Here the following approach is chosen,

$$\widehat{\Delta\phi_m^a} = \text{median}(\widehat{\Delta\phi_m}(t,\omega)) \tag{16}$$

for $t_0^a - \frac{3}{2}\lambda \le t \le t_0^a + \frac{3}{2}\lambda$ and $\omega_0^a - \pi/2\lambda \le \omega \le \omega_0^a + \pi/2\lambda$ where $(t_0^a, \omega_0^a)$ is the maximum of the cross-spectrogram calculated with Gaussian window as in (15). We define this method as Reassignment Vector Phase Difference Estimator (RVPDE).

The reason for taking the median is that the shape of the complex distribution $F_z^{th}/F_z^h$ for a signal $z(t) = x(t) + n(t)$, where $n(t)$ is white noise, is non-Gaussian. This result was analytically derived in [17] and extended in [18]. Thus, either $\Re(F_z^{th}/F_z^h)$ or $\Im(F_z^{th}/F_z^h)$ risks not being Gaussian distributed, as can be seen in an example signal in Figure 2. Consequently the sum in (13) will not be necessarily Gaussian distributed when there are high levels of noise. The median compared to the mean will not be as biased towards the tail of the distribution.

A mixture of components in the cross-spectrogram leads to joint components with unknown characteristics and thus RVPDE estimates become unstable over such bins, see Figure 1. Using longer or shorter window can mitigate this effect if components are close in either frequency or time respectively.

## V. Simulation & Evaluations

### A. Pixel dependance on noise

As an initial measure of how the phase difference estimates of RVPDE behaves in a single TF-bin in the presence of noise, Gaussian envelope signal components with TF centre $(t_0 = 100, \omega_0 = \pi/2)$, of length 200, with $\sigma = 12$, $\phi_0 \in U[0, 2\pi]$ and $\Delta\phi \in U[\pi/8, 3\pi/8]$ are simulated with disturbances by white Gaussian noise of variance $\sigma_e^2$. The boundary of $\Delta\phi$ is chosen to reduce the effects of phase wrapping on analysis. Figure 3a shows a histogram of the errors of $\widehat{\Delta\phi}(t,\omega)$ from 1000 realizations with $\sigma_e^2 = 1$, $\lambda = 12$

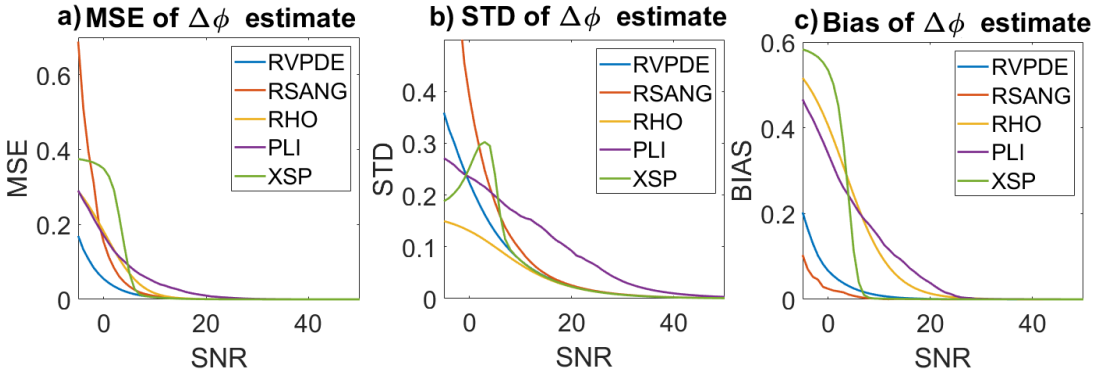


Fig. 4. (a), (b) and (c) show mean square error (MSE), STD and bias respectively of error of $\widehat{\Delta\phi_m^a}$ for the presented method RVPDE Reassigned Spectrogram Angle (RSANG), Pearson's linear correlation (RHO), Phase Lag Index (PLI) and cross-spectrogram phase (XSP) evaluated over multiple SNR-values.

in one bin chosen at $(t, \omega) = (t_0, \omega_0 + 10\pi/512)$, a slightly higher frequency than the centre of signal component. The errors are approximately normally distributed which is true for $\sigma_e^2 \leq 2$. However for $\widehat{\Delta\phi_m}(t, \omega)$ the errors will have an shifted, non-normal distribution which is problematic.

This problem is accentuated with increasing $\sigma_e^2$ of noise, and additionally motivates why taking the median of the area in RVPDE in section 4 is a suitable choice if a method robust to high power of noise is desired. Figure 3b shows a plot of estimated variance of errors against the power/variance of added signal noise. As one can see the variance of errors increase linearly with power of noise up to a certain level. This is a maximum since the variance of errors can at most be a distribution still on the interval $[0, 2\pi]$.

### B. RVPDE compared to commonly used methods

To measure the performance of RVPDE compared to other commonly used methods for phase difference extraction a single Gaussian shaped component signal $x(t)$ defined at 200 samples with $t_0 = 100$, $\omega_0 = \pi/2$, $\phi_0 \in U[0, 2\pi]$, $\sigma = 12$ and average power $P = \int_{t_0-3\sigma}^{t_0+3\sigma} x(t)^2\, dt/6\sigma = 1$ was used. Two channels $y_1(t)$ and $y_2(t)$ were constructed according to (7) with $\Delta\phi \in U[\pi/8, 3\pi/8]$. White Gaussian noise at multiple SNRs, defined as SNR$= 10\ \log_{10}(P/\sigma_e^2)$, was added. As an example, the $\sigma_e$ in Figure 1 corresponds to SNR$= -6$. Simulations were performed 1000 times.

For the novel method RVPDE a Gaussian window with $\lambda = 12$ was applied. To compare the method with previous developed methods, four other methods are evaluated: Reassigned Spectrogram Angle (RSANG) based on (11) and (12) using identical window as RVPDE but with other assertions on the shape of component envelope [16], Phase Lag Index (PLI) [19], Pearson's linear correlation (RHO) and TF cross-spectrogram phase (XSP) [1]. For PLI and RHO the measures were reduced to the temporal interval of $\pm 2.5\lambda$ from component centre to improve the performance of these methods. The cross-spectrogram for XSP is calculated using the same window as in RVPDE. The mean-square-error (MSE), standard deviation (STD) and bias of $\widehat{\Delta\phi}$ for all methods are shown in Figure 4.

RHO and PLI behave similarly and even though signals were cropped to improve the performance of these methods they still perform the worst. XSP shows a good performance for SNR $> 4$ but at the boundary bias and STD increase drastically. RSANG and RVPDE, have very similar performances at higher SNRs. At lower SNR RSANG exhibits a lower bias, and in turn a powerful increase in STD as SNR decreases below 1. RVPDE has instead a superior STD with a slightly increased bias instead. Overall the MSE shows a substantial improvement for the novel RVPDE at low SNR compared to the RSANG and state-of-the-art methods.

### C. Resolving TF-spatially close components

The robustness of RVPDE to the mixing of components in the TF-plane is evaulated by simulating the signal pair $y_1(t)$ and $y_2(t)$ as defined in section 5.2, but with two-component signals, a component of interest $a$ and a disturbance component $b$. The two Gaussian components have $\sigma^a = \sigma^b = 12$, $t_0^a = t_0^b = 100$ and the same power. Furthermore $\phi_0$ and $\Delta\phi$ share the uniform distributions from section 5.2 for both component $a$ and $b$ but are independently realised. Frequency centres are defined as $\omega_0^a = 2\pi/4$ and $\omega_0^b = 2\pi/4 + \Delta\omega$ where $\Delta\omega = k\omega_0$, $k = 0, 0.05, 0.1, ..., 0.4$ and the signal is realised 1000 times at SNR$= 1$ with white Gaussian noise.

STD and bias for $\widehat{\Delta\phi_m^a}$ by RVPDE with a matched window ($\lambda = \sigma$), a shorter window ($\lambda = \sigma/2$) and a longer window ($\lambda = 2\sigma$) are shown in Figure 5. One can see in Figure 5 that increasing the width of the window used in RVPDE decreases acceptable $\Delta\omega$ before bias and STD of errors increase substantially. A tunability of RVPDE for investigating components of particular frequency and shape is made possible by this characteristic. An analogue simulation with temporally close components will show a opposite relation for the robustness of RVPDE. In this case shorter windows will increase the robustness with regards to temporally close components.

## VI. Example with real data

As real data example of the application of phase difference estimation of visually evoked potential (VEP) EEG generated from a flickering light of 20 Hz presented to the subject is examined. Electrodes were spaced according to the 10-20

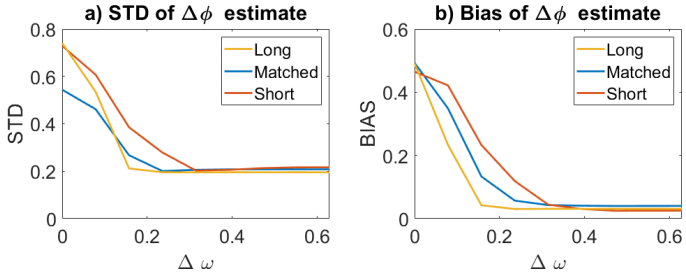


Fig. 5. a) STD and b) bias of phase difference estimates of a main component in a signal pair also containing a second disturbance component as a plot against decreasing frequency separation $\Delta\omega$, for multiple window lengths in RVPDE.

system at positions Fp1, Fp2, F3, F4, C3, C4, P3, P4, O1, O2, F7, F8, T3, T4, T5, T6, Fz, Cz, Pz, Pg1 and Pg2. Oscillations of 20 Hz are expected at the optical cortex, and propagate forward through the scalp. $O_2$ is placed to the right of the optical cortex and a positive phase difference lag to other electrodes should in theory be observed.

Data, with a length of 15s, was captured at a sample rate 256 Hz, with flickering light between 5 and 10 seconds. Before analysis, data was temporally cut to the range of the flickering light (5-10s). Data was normalized over the remaining 5s to equate component amplitudes in each channel. The evaluation is restricted to RVPDE, RSANG and PLI as the other methods failed to perform in interpretable ways. The results of RVPDE and RSANG were calculated with $\lambda = 12$ and component centres were chosen manually as the strongest peak in the cross-spectrogram for $O_2$ channel in the frequency band 18-22 Hz. For PLI the signal was cropped to $\pm 3\lambda$ from the empirically found peak. Figure 6 shows phase estimates $\widehat{\Delta\phi}$ between $O_2$ and the electrode in examination. PLI seems to capture a reasonable phase difference with a delay lag from $O_2$. However RVPDE estimates larger positive phase differences, whereas RSANG completely fails to capture these expected positive phase differences.

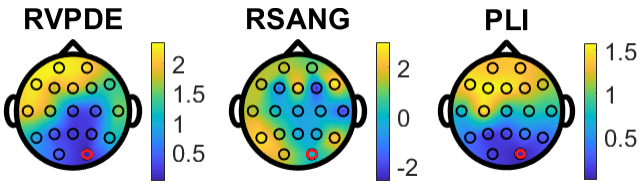


Fig. 6. Topographic map of channels showing estimated phase difference using methods RVPDE, RSANG and PLI. Red circle shows $O_2$ electode.

## VII. Conclusion

We have presented the novel RVPDE method for robust multi-channel phase difference estimation at low SNRs. The RVPDE outperforms commonly used methods within EEG in terms of mean square errors for SNRs $< 5$. The advantages of RVPDE are that the method is not restricted to specific spectrogram window shapes and does not make any assumptions regarding the envelope shapes of components. Therefore the applied spectrogram window can be adjusted for higher performance in presence of TF-spatially close disturbance components. Future approaches aim to utilize multitaper reassignment techniques and exploration of RVPDE phase estimates in feature based machine learning models.

## References


[1] L. Cohen, *Time-Frequency Analysis*, Signal Processing Series. Prentice-Hall, Upper Saddle River, NJ, USA, 1995.

[2] F. Auger and P. Flandrin, "Improving the readability of time-frequency and time-scale representations by the reassignment method," *IEEE Trans. on Signal Processing*, vol. 43, pp. 1068–1089, May 1995.

[3] I. Daubechies, J. Lu, and H.-T. Wu, "Synchrosqueezed wavelet transforms: An empirical mode decomposition-like tool.," *Applied & Computational Harmonic Analysis*, vol. 30, no. 2, pp. 243 – 261, 2011.

[4] J. Zhang, D. Yang, W.-X. Ren, and Y. Yuan, "Time-varying characteristics analysis of vehicle-bridge interaction system based on modified S-transform reassignment technique.," *Mechanical Systems and Signal Processing*, vol. 160, 2021, 107807.

[5] D. Fourer, F. Auger, and G. Peeters, "Local AM/FM parameters estimation: Application to sinusoidal modeling and blind audio source separation," *IEEE Signal Processing Letters*, vol. 25, no. 10, pp. 1600–1604, 2018.

[6] E. M. Månsson and M. Sandsten, "The smoothed reassigned spectrogram for robust energy estimation," in *Proceedings of the EUSIPCO*, Amsterdam, Netherlands, 2020, Virtual.

[7] Y. Wang, Y. Bai, X. Xia, Z. Niu, Y. Yang, J. He, and X. Li, "Comparison of synchrosqueezing transform to alternative methods for time-frequency analysis of TMS-evoked EEG oscillations.," *Biomedical Signal Processing and Control*, vol. 70, 2021, 102975.

[8] M. Hansson-Sandsten and J. Brynolfsson, "The scaled reassigned spectrogram with perfect localization for estimation of Gaussian functions," *IEEE Signal Processing Letters*, vol. 22, no. 1, pp. 100–104, 2015.

[9] J. Brynolfsson and M. Sandsten, "Parameter estimation of oscillating Gaussian functions using the scaled reassigned spectrogram," *Signal Processing*, vol. 150, pp. 20–32, 2018.

[10] J. Brynolfsson, I. Reinhold, and M. Sandsten, "A time-frequency-shift invariant parameter estimator for oscillating transient functions using the matched window reassignment," *Signal Processing*, vol. 183, 2021, 107913.

[11] S. Sumitani, R. Suzuki, N. Chiba, S. Matsubayashi, T. Arita, K. Nakadai, and H. G. Okuno, "An integrated framework for field recording, localization, classification and annotation of birdsongs using robot audition techniques - harkbird 2.0.," *ICASSP*, pp. 8246 – 8250, 2019.

[12] B. He, L. Astolfi, P. A. Valdés-Sosa, D. Marinazzo, S. O. Palva, C.-G. Bénar, C. M. Michel, and T. Koenig, "Electrophysiological brain connectivity: Theory and implementation," *IEEE Trans. on Biomed. Eng.*, vol. 66, no. 7, 2019.

[13] J. L. Busch, L. K. Feldmann, A. A. Kühn, and M. Rosenblum, "Real-time phase and amplitude estimation of neurophysiological signals exploiting a non-resonant oscillator.," *Experimental Neurology*, vol. 347, 2022.

[14] M. Sandsten, R. Anderson, I. Reinhold, and J. Brynolfsson, "The matched reassigned cross-spectrogram for phase estimation," in *Proceedings of the ICASSP*, Barcelona, Spain, 2020, IEEE, Virtual.

[15] M. Sandsten, R. Anderson, I. Reinhold, B. Bernhardsson, C. Bergeling, and M. Johansson, "A novel multitaper reassignment method for estimation of phase synchrony," in *Proceedings of the EUSIPCO*, Dublin, Ireland, 2021, Virtual.

[16] M. Sandsten, I. Reinhold, and R. Anderson, "Parameter estimation from the cross-spectrogram reassignment vectors," in *Proceedings of the EUSIPCO*, Dublin, Ireland, 2021, Virtual.

[17] E. Chassande-Mottin, P. Flandrin, and F Auger, "Statistique des vecteurs de reallocation du spectrogramme," Rapport interne, Laboratories de Physique, ENS-Lyon (URA 1325 CNRS), Lyon (France), 1 1996.

[18] E. Chassande-Mottin and P. Flandrin, "On the statistics of spectrogram reassignment vectors," *Multimedia Systems and Signal Processing*, , no. 9, pp. 355–362, 1997.

[19] C. J. Stam, G. Nolte, and A. Daffertshofer, "Phase lag index: Assessment of functional connectivity from multi channel EEG and MEG with diminished bias from common sources.," *Human Brain Mapping*, vol. 28, no. 11, pp. 1178–1193, 2007.